Sudan University of Science and Technology

College of Graduate Studies

Impact of Annealing Temperature and Silver Concentration on the Formation of Silver Nanoparticles in Silica

تاثير درجة حرارة التلدين وتركيز الفضة في تكوين جسيمات الفضه النانوية في السليكا

A dissertation Submitted in Partial Fulfillment for the Requirement of a Master degree (M. Sc.) in Physics

Prepared by:

Walaa Musa ELkheir Abdalla

Supervised by:

Dr. Abd Ellateef Abbass

December 2020

Acknowledgements

Firstly, I'd like to express my thanks to my patient and supportive supervisor Dr. Abd Ellateef Abbass for providing guidance and feedback throughout this project. Also, my thanks goes to University of The Free State for providing us with samples that we work in. Also, I would like to thank the following people, without whom I would not have been able to complete this research, and without whom I would not have made it through my master degree, my colleagues Talal, Ahmed and Sara at Sudan University of Science and Technology.

Finally, I would like to thank my family for supporting me during the compilation of this dissertation.

Abstract

The optical and structural properties of silica doped with silver were investigated in detail at various annealing temperatures (from 500 °C up to 1300 °C) and silver concentration (from 0.1 - 5 mol%). To investigate the effects of Ag concentration and annealing temperature on the formation of silver nanoparticles, complementary techniques were used namely ultraviolet-visible spectrometer (UV-VIS), X-ray diffraction (XRD), scanning electron microscopy (SEM) and transmission electron microscopy (TEM).

The obtained results showed that the crystalline phase of silver did not form in samples annealed below 800 °C while for annealing temperature above 1000 °C the amount of silver is reduced by evaporation. This indicates that the optimum annealing temperature is in between 800 °C-1000 °C.

It is also revealed that the size of silver nanoparticles is increases with increasing the annealing temperature while increasing of Ag concentration had no significant effect on the particle size. It is also found that the peak intensity of the XRD pattern related to silver was increases as function of silver loads up to 1mol% and then decreased, indicating that the optimum concentration of silver is about 1mol%. On the other hand, it is found that the increasing of Ag loads in silica is catalyzed the structure order of amorphous silica towards the cristobalite phase.

المستخلص

تم التحقق من الخواص البصرية و التركيبية للسليكا المشوبة بالفضة عند درجات حرارة مختلفة (500 درجه مئوية الي 1300 درجه مئوية) و تراكيز مختلفة للفضة (0.1 مول % الي 5 مول %). لدراسة تأثيردرجة حرارة التلدين و تركيز الفضة علي تكوين جسميات الفضة النانوية ،تم استخدام عدد من الأجهزة مثل مقياس الطيف للأشعة فوق البينفسجيه، حيود الاشعة السينية، المجهر الإلكتروني الماسح و المجهر الإلكتروني النافذ.

أوضحت النتائج المُتحصل عليها أن الطور البلوري لا يتكون في حالة العينات التي تمت معالجتها عند درجات حرارة تلدين أقل من 800 درجة مئوية في حين أن كمية الفضة في السليكا نقصت عند تسخين العينة في درجة حرارة أعلى من 1000 درجة مئوية نتيجة لتبخر الفضة و هذا يشير إلى أن درجة حرارة التلدين المثلى لتكوين جسيمات الفضة النانوية تتراوح بين 800-1000 درجة مئوية.

أيضا اوضحت النتائج أن حجم جسيمات الفضة النانوية يزيد بزيادة درجة حرارة التلدين بينما زيادة تركيز الفضة ليس له أي تأثير يذكر علي حجم جسيمات الفضة النانوية. كذلك وُجد أن شدة ذروة نمط مقياس حيود الاشعة السينية للفضة يزيد بزيادة تركيز الفضة حتي 1 مول% ثم ينقص بعد هذا التركيز، مما يشير الي أن التركيز المثالي للفضة هو 1 مول%. من جانب آخر وجد أن زيادة تركيز الفضة يحفز ترتيب بنية السيليكا غير المتبلورة باتجاه مرحلة أو بنية بلورية متميزه.

Keywords and Acronyms

Keywords

Silver NPs - Optical and Structural properties - Surface Plasmon Resonance – Localized Surface Plasmon Resonance.

Acronyms

Ag NPs: Silver Nano particles.

SPR: Surface Plasmon Resonance.

SPP: Surface Plasmon Polartion.

LSPs: Localised Surface Plasmon.

LSPR: Localized Surface Plasmon Resonance.

UV: Ultra Violet.

XRD: X- Ray Diffraction.

TEM: Transmission Electron Microscopic.

FWHM: Full Width at Half Maximum.

EDX: Energy Dispersive X-ray

EELS: Electron Energy Loss Spectroscopy

SEM: Scanning Electron Microscopic.

Table of Contents

CHAPTER TWO

THEORETICAL BACKGROUND

CHAPTER THREE

METHOD AND TECHNIQUES

CHAPTER FOUR

RESULTS AND DISCUSIONS

List of Figures

List of Tables

CHAPTER ONE

INTRODUCTION

1.1 Overview

In the last century, the word "Nano" has attracted many scientists and it has been mentioned in several research fields such as chemistry, physics, medicine and biology (Ning, S., 2012). Nanometer is refers to a unit of measurement and by definition it is about one billionth of a meter ($10^{-9}m$). Actually, there are two fields of research associated with the nanoscale namely, nanoscience and nanotechnology. Nanoscience is defined as the field of research that studying and manipulating materials in nano scale while nanotechnology is refers to field of applied science focused on the design, synthesis, characterization and applications of materials at nanoscale (Prema, P., 2011).

Recently, noble metals nanoparticles (NPs) have gained more attention due to their fascinating chemical, physical and biological properties. Due to these promising properties, noble metal NPs have found wide range of applications in several areas, including nonlinear optical devices, surface-enhanced Raman spectroscopy, near-field scanning optical microscopy, sensing, waveguides made of nanoparticle chains, in solar cells, light--emitting diodes and integrated optics (Ojeda-MartÍnez, M. L., et al., 2013). Moreover, metal NPs dispersed in dielectric materials exhibit a strong characteristic extinction peak, due to physical phenomenon called localized

surface plasmon resonance (LSPR). Plasmon is defined as the collective oscillations of the conduction electrons in metals NPs. The collective oscillation of these electrons leads to a resonant interaction when the frequency of incident light matches their natural frequency which is called LSPR (Matthew, R., et al., 2011). Depending on the dimension of metal NPs (small NPs), the free electrons in these NPs oscillates transforming energy from light into thermal energy in an absorption process while for relatively large NPs these electrons can be accelerated transforming energy into scattering process (Matthew, R., et al., 2011). Of interest is that the LSPR is greatly enhanced electric field near the NPs surfaces in both cases of absorption (near field enhancement) and scattering (far field enhancement). Therefore, the most applications of the LSPR are associated with electric field enhancement (near field or far field enhancement) (Kamal, K. P. and Pravat, K. G., 2017). Surface-enhanced Raman spectroscopy and near-field scanning optical microscopy are examples for far field enhancement and near field enhancement, respectively (Renata, R., et al., 2011).

Among noble metal NPs, Silver nanoparticles (Ag-NPs) are gained high scientific and economic interest due to their wide range of applications in several technological fields such as biology, medicine, material science and etc. Moreover, silver NPs is known to have high biological efficiency even at low concentration and therefore it intensively used as antimicrobial agents and against a broad range of germs like bacteria (Mahltig, B., et al., 2009).

It is important to note that the size, shape and the distribution of Ag-NPs in different hosts particularly in silica are played an important role in their application in all most all fields of research. Although there are lots of research about Ag-NPs doped silica glass, still there are lack information about the effect of annealing temperature and concentration on the formation of Ag-NPs and their optical and structural properties. Therefore, in this work, the effect of wide range of annealing temperature and concentration on the formation of Ag-NPs in silica and their optical and structural properties will be investigated. In addition, different complementary characterization techniques will be applied in order to compare the results.

1.2 Literature Review

Composite materials containing nanoscale particles of transition metal like Ag embedded in glass as the dielectric matrix are of great interest and have been a subject of intense research due to their unique optical characteristic and their fascinating surface Plasmon resonance (SPR) properties. For example Jyotia Rozra et.al reported theoretical and experimental studies of structural and optical properties of Ag-NPs in glass using different techniques (UV-visible, XRD and TEM). The samples were annealed at various temperatures from 300^{o}C to 550 ^{o}C. the obtained results showed LSPR peak around 427nm which confirmed the formation of silver nanoparticles. They also found that the size of Ag-NPs is increased by increasing of annealing temperature (Jyoti, R., et al., 2013). Furthermore, F.Y Alzoubi and S.A. Abu Bidier reported synthesis of silver NPs using chemical reduction method. The average diameter of Ag-NPs was estimated using the results obtained from UV-Vis and TEM techniques and found to

be about 68 nm (Alzoubi, F. Y, et al., 2012). In addition, Mauro Epifani et.al., reported synthesis of silver and gold NPs using sol-gel process in SiO_2 thin films. The obtained results from XRD showed that the intensity, the broadness of peak and the particles sizes were increased with increasing annealing temperature (Mauro, E., et al., 2000). Recently, Farasat, M., were studied the crystallinity of silver nanoparticles according to their XRD patterns. Three peaks were recognizable at Bragg angles of 38.10, 44.33 and 64.42. The average crystallite size was calculated and found to be about 18 nm (Farasat, M., et al., 2011).

1.3 Problem Statement

Recently, silica doped with silver NPs has become more and more popular due to increasing of its applications in almost all fields. Most of these applications depend on their structural and optical properties. These properties are actually depends on the sizes and shapes of Ag-NPs and their distribution in silica. According to literature, there are many parameters that have been used to control the formation of Ag NPs in silica particularly annealing temperature and concentration. Therefore, in this work wide range of annealing temperature and concentration is used and different characterization techniques are applied to highlights the effect of these two parameters on the formation of Ag-NPs in silica and their structural and optical properties.

1.4 Research objective

1.4.1 General Objective

To investigate the effect of annealing temperature and silver concentration on the formation of Ag-NPs in silica and their structural and optical properties

1.4.2 Specific Objectives

- To use experimental data to calculate the size of silver nanoparticles.
- To determine peaks intensity for all samples at different concentration and temperature using x-ray diffraction (XRD).
- To use obtained data from UV-visible to confirm the formation of Ag NPs.
- To determine peaks position and calculate the full width at half maximum (FWHM) for all samples and at various concentration and temperature.
- To characterize NPs from SEM and TEM measurements, determine the shape and to calculate the particle sizes.
- To compare the obtained results from SEM and TEM with the results obtained from XRD and UV-visible.

1.4 Dissertation layout

This dissertation consists of five chapters as follow: Chapter one provides general information and the aim of this work. Chapter two focus on the theoretical background. The methodologies that used in this work were discussed in chapter three. The results and discussion were presented in chapter four, while the conclusion and the future work were given in chapter five, lastly list of references.

CHAPTER TWO

THEORETICAL BACKGROUND

2.1 Silver Nanoparticles

Nanoparticles exhibit size and shape-dependent properties which are of interest for several applications. Silver nanoparticles are of interest due to their unique properties such as size and shape depending optical, electrical, and magnetic properties, which can be incorporated into antimicrobial applications, biosensor materials, composite fibers cryogenic superconducting materials, cosmetic products, and electronic components (Tanja, K., et al., 2001). Silver nanoparticles have drawn the attention because of their extensive applications in areas such as integrated circuits (Stefan, K., et al, 1997), sensors, biolabelling and filters (Guozhang, C., 2004) and antimicrobial deodorant fibres (Feng, W. and Ron-Shen, Y., 2003). Silver nanoparticles have been used as antimicrobial agents in health industry, food storage and textile coatings and in enormous environmental applications. Antimicrobial properties of silver nanoparticles caused the use of these nanometals in different fields of medicine. For instance, it was shown that silver nanoparticles mainly in the range of 1-10 nm attached to the surface of *E. coli* cell membrane and disturbed its proper function (Jose, R. M., et al., 2005). In general, the effects of silver particles depend on important aspects, such as particle size (surface area and energy), particle shape (catalytic activity), particle concentration (therapeutic index) and particle charge (oligodynamic quality) (Sukdeb Pal, et al., 2007). Therefore,

designing and production of materials with novel applications can be resulted by controlling shape and size at nanometer scale.

2.2 Plasmon

Nanostructured metals show very complex and interesting optical properties. The most striking phenomenon encountered in these structures is electromagnetic resonances due to collective oscillations of the free conduction electrons due to an external electric field termed Plasmon. Plasmon modes exist in a number of geometries and in various metals, most importantly in noble metals such as gold and silver. The boundary conditions for electromagnetic fields lead to different conditions for the occurrence of Plasmons for the cases of bulk material, planar metal-dielectric interfaces and metal particles. Therefore, it is useful to distinguish these modes by speaking of bulk, surface or particle Plasmons, respectively in the following sections.

2.2.1 Bulk Plasmon

In bulk metals at equilibrium state and when there is an external field applied, the free electrons will make longitudinal oscillations through the metal. These oscillations occur at certain frequency called plasma frequency ω_p and is given by (Nicholas, J. B., 2011):

$$\omega_p = \sqrt{\frac{ne^2}{\epsilon_0 m}} \qquad (2.1)$$

where n is the electrons density, e and m are charge and mass of electron respectively and ϵ_0 is the permittivity of free space.

Bulk Plasmon cannot be excited by photon due to the miss matching between longitudinal oscillation of free electrons in metals and transverse oscillation of light. Thus, instead of photon, electrons beam is used to excite the bulk Plasmon (see figure (2.1)) (Vincenzo, A., et al., 2017).

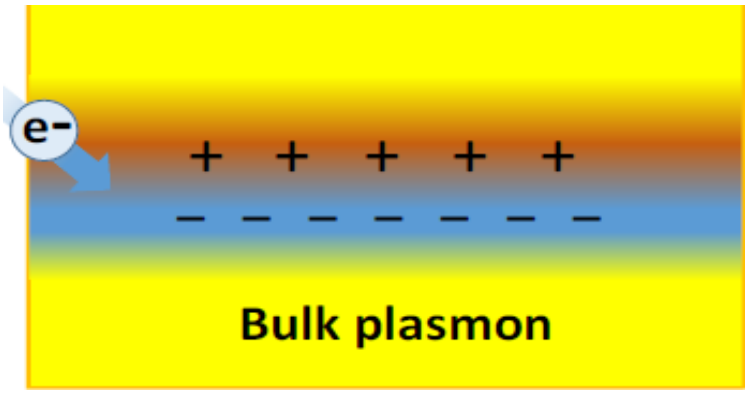

Figure 2.1 Schematic diagram illustrating Bulk Plasmon

2.2.2 Surface Plasmon

Surface plasmons are electromagnetic modes bound to metal-dielectric interfaces, involving charges in the metal and electromagnetic fields in both media. The field intensity in the metal as well as the dielectric medium falls off exponentially in the direction normal to the surface. In the plane of the interface, the field intensity and charge distribution in the metal propagates as a longitudinal wave along the surface. By another word is an optical phenomenon arising from the collective oscillation of conductive electrons in a metal when the electrons are disturbed from their equilibrium positions (Xianmao, L., et al., 2009). There are two modes of surface Plasmon that metal can support, one is localized at the metal nanoparticle called localized surface Plasmon (LSP) and another is propagating at the interface between

metal and dielectric called surface Plasmon polaritons (SPP) (Matthew, E. S., et al., 2008). The following sections will give details about these modes.

2.2.2.1 Localized surface Plasmon

Localized surface Plasmon is a phenomena occurs in metals nanoparticles having dimensions much smaller than the wavelength of incident light($R \ll \lambda$).When metal particles exposed by light, the electric field of the incident light induced an electric dipole in the metal particles. Since the charge distribution counts on the electric field orientation, many surface electron moves to one side of the metal particles leaving a net positive charge on the other side as shown in figure (2.2) and when the oscillation frequency of electrons match the frequency of incident light, resonance is set up resulted in strong absorption band in the visible region of electromagnetic spectrum (Matthew, R., et al., 2011).

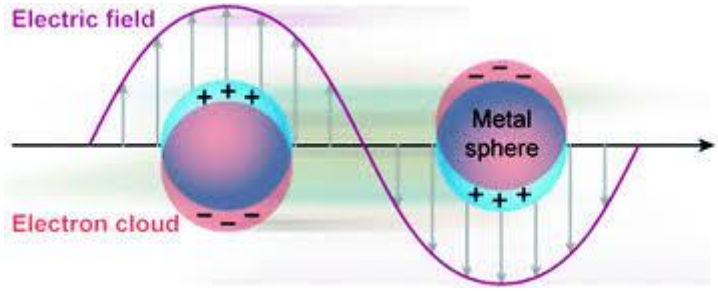

Figure 2.2 Schematic diagram illustrating localized surface Plasmon.

The resonance frequency (position of absorption band of LSPR) depends on various factors such as the type of metal, sizes and shapes of NPs.

2.2.2.2 Surface Plasmon Polariton (SPP)

A surface plasmon polariton is an electromagnetic excitation existing on the surface interface between dielectric and metals. It is an intrinsically two-dimensional excitation whose electromagnetic field decays exponentially

with the distance from the surface (Anatoly, V. Z., et al., 2005). Propagating surface Plasmon (Surface Plasmon Polariton**)** does not produced unless the momentum of electric field associated to incident light is matches to the surface plasmon of metal (coupling between Plasmon and photon) (Ning, S., 2012). As the results, some optical apparatus such as glass prism are used to manipulate the momentum of photons. Figure 2.3 showed the propagating surface Plasmon polariton.

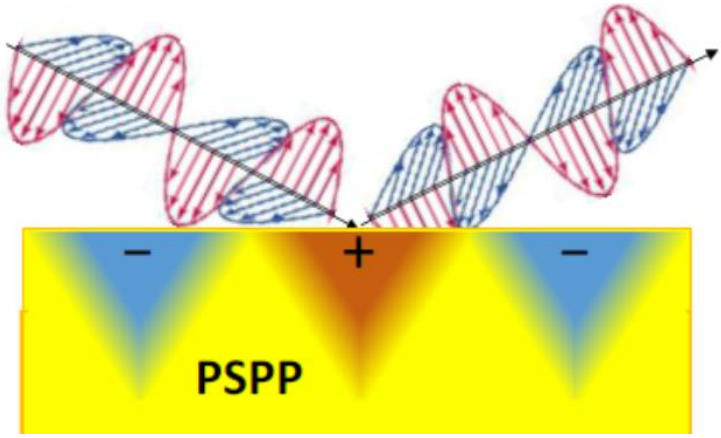

Figure 2.3 Show the propagating surface Plasmon polariton (Vincenzo Amendola, et al., 2017**).**

2.3 Tuning of the Localized Surface Plasmon Resonance

Nanoparticles show fascinating properties with unusual characterization that lead to the formation of unique properties in nanosystems. Additionally metallic NPs with sizes smaller than the wavelength of the light show localized surface plasmon resonance (LSPR), the resonance frequency of the oscillation and the surface plasmon energy are determined by the particle size and shape and the dielectric environment (Rivera, V.A.G., et al., 2012). The following sections will explore the effect of those parameters.

2.3.1 The Effect of Size

Metal nanoparticles absorb and scatter light at plasmon resonance frequency, the size of nanoparticles determines plasmonic features and how other physical parameters affect the LSPR. Therefore, size is an important variable that must be considered to discuss about plasmonic properties (Carsten, S., 2001).

For small particles ($R \leq 30$) absorption dominate over scattering while on other hand larger particles can scatter light more efficiently. Matthew Rycenga et al discussed about the dependence of the number of LSPR absorption band based on the nanoparticles size. The obtained results showed that for small particles there is only dipole excitation whereas for large particles both dipole and multipole excitation are possible. It is also found that as the size increased the charge separation increase leading to lower frequency for the collective oscillation of electrons and thus red-shift the absorption wavelength (Matthew, R., et al., 2011).

2.3.2 The Effect of Shape

The shape of nanostructures can have a large effect on their LSPR properties. M. Rycenga et al calculate the extinction spectra for Ag nanostructure with various geometrical shapes (sphere, cube, octahedron and right pyramids) and observed that the number of resonances increase as the symmetry decreased. As can be seen in figure 2.4 and in general structure with sharp features tend to increase charge separation and reduce the restoring force for dipole oscillation thus they have red-shifted peaks (Matthew, R., et al., 2011).

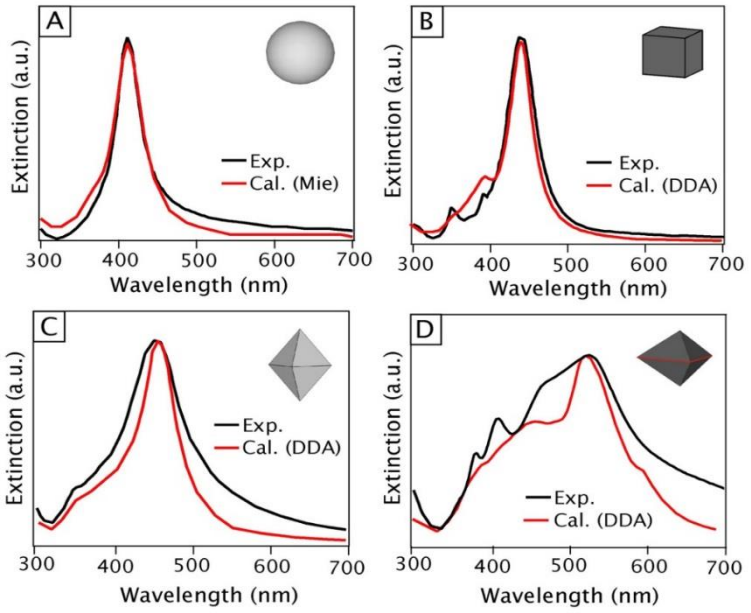

Figure 2.4 shows the effect of the shape on the LSPR peak (Matthew, R., et al., 2011)

2.3.3 The Effect of Dielectric

The dielectric environment has significant impact on the LSPR properties. The LSPR profile for a given metal can be modified by its environment by means of dielectric constant ε_m and this because of the sensitivity of excitation cross-sectional spectrum to the value of dielectric constant as can be seen in the following equation.

$$C_{ext} = \frac{18\pi\,[\varepsilon_m(\lambda)]^{\frac{3}{2}}}{\lambda}\, V_{NPs}\, \frac{Im[\varepsilon(\lambda)]}{[Re(\varepsilon) + 2\varepsilon_m(\lambda)]^2 + Im[\varepsilon(\lambda)]^2} \qquad (2.3)$$

where V_{NPs} is volume of nanoparticle, ε_m is dielectric function of surrounding medium, $Re(\varepsilon)$ and $Im(\varepsilon)$ are the real and imaginary part of dielectric function, respectively, λ is the wavelength of the incident light

Salem Marhaba calculated the extinction cross sections for silver nanoparticles with a diameter of 20nm in different environment (vaccum,

silica and alumina) and it is clear that the spectral position will move to red by increasing ε_m as shown in Figure 2.5 (Salem, M., 2018).

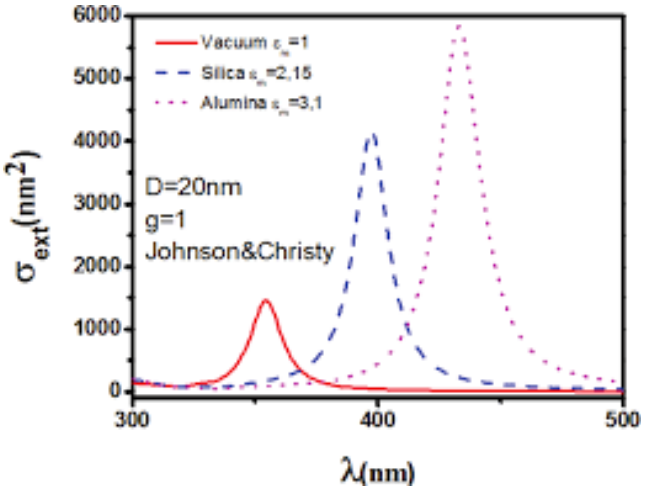

Figure 2.5 shows Extinction cross sections for a silver nanoparticle with a diameter of 20 nm calculated by the quasi-static approximation in different environments: Vacuum $\varepsilon_m = 1$, silica $\varepsilon_m = 2.15$ and $\varepsilon_m = 3.1$

CHAPTER THREE

METHOD AND TECHNIQUES

3.1 Method and materials

All samples were prepared and characterized at the University of the Free State, South Africa.

Pure silica (SiO_2) doped with Ag were synthesized using sol gel method. The starting materials used to prepare these samples consisted of distilled water, ethanol (C_2H_5OH ,99.0%) and tetraethylorthosilicate (TEOS, 99.7%) with molar ratio taken to be 1:5:10 for TEOS: ethanol: water respectively

(Abbass, AE., et al., 2017). Silver nitrate (Ag NO_3, 99.9%) was used as the source of Ag. For all samples, TEOS was dissolving in ethanol by using magnetic stirring for 30 min. After that dilute HNO_3 (0.15 M) was added to the solution instead of water and stirred for another 30 min. To dope the silica, Ag NO_3 was dissolved first ultrasonically in small amount of dilute HNO_3 and then added to the mixture which was stirred for further 5 h. The gel was achieved by placing the solution in closed container and storing in a water bath at 50 °C for 24 h, then dried in opened container in air for 24 h and then ground to fine powder and annealed in air at different temperatures for 2 h.

A brief description of the characterization techniques that used in this study namely UV-Vis spectrometer, X-ray diffraction, Transmission electron microscope and scanning electron microscopy will be presented in the next sections.

3.2 X-ray Diffraction (XRD)

X-ray diffraction is analytical technique used for phase identification of a crystalline materials, provides information on unit cell dimension and to study crystal structures. The basic geometry of X-ray diffractometer consist a source of monochromtic radiation and X-ray detector situated on the circumference of a graduated circle centered on the powder sample. There are two divergent slits one located between the source of X-ray and another between the sample and detector, limit scattered radiation to reduce the background noise and collimate the radiation. The detector and specimen holder are coupled with a gonionmeter (Poppe, L. J., et al, 2001).

X-ray diffraction is depend on the interference of X-ray and crystalline sample. As shown in figure 3.1, X-rays are generated in a cathode tube by heating to produce electrons and by applying a voltage the electrons accelerated toward a target, the specific wavelength is characteristic of target material. The commonly used material are Cu, Fe, Mo and Cr but the copper is most common one with λ=0.154nm. If electrons have enough energy dislodge the inner shell of the sample, X-ray spectra were produced. These X-ray are directed to the sample, if the sample and detector are rotated, the intensity of reflected X-rays is recorded. The constructive interference occurred when Bragg Equation ($n\lambda=2d\ sin\ \theta$) is satisfied (Barbara, L. D., et al., 2018).

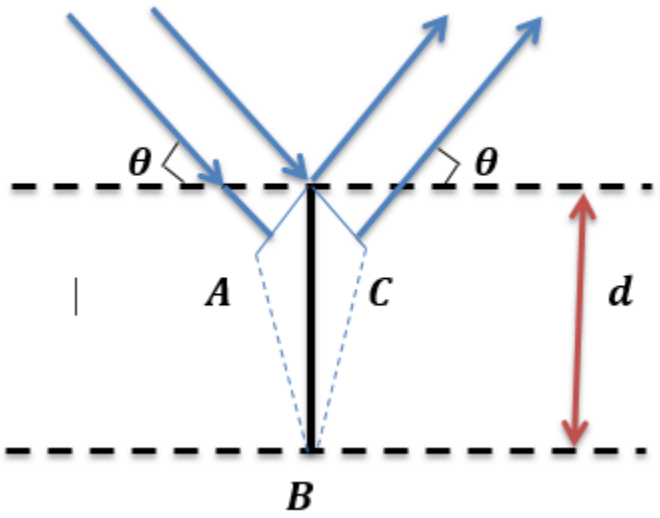

Figure 3.1. The diffraction of X-ray beams from crystal

X-ray diffraction is a common and powerful nondestructive technique for characterizing crystalline materials. It provides information on phases,

structures, texure and other structural parameters such as average grain size, strain, crystallity and crystal defects (Andrei, A. B., et al., 2015).

The crystallite size is determined by using Sherrer equation:

$$D = \frac{K\lambda}{(\beta \cos \theta)} \qquad (3.1)$$

Where K is a constant and used to be 0.9 in case of spherical shape, β is full width at half maximum (FWHM) in radians, θ is Bragg angle at which the peak maximum occurs and λ is the wavelength of X-ray radiation used in this study, λ = 0.154 nm .

3.3 Transmission Electron Microscope (TEM)

TEM is an analytical tool and a microscopy technique used to examine the structure, properties, composition of samples and to study biological and medical materials (Ping-Chang, L., et al, 2014).

Figure 3.2 shows the components and principle of TEM, the first part of TEM contains the source of electrons that usually a V-shaped filament, condenser lens to focus the steam of electrons to small coherent beam, condenser aperture used to restrict electrons and filter out unwanted scattered electrons prior image formation, sample, objective lens to focus transmitted electrons from the sample and into an image, enables to examine the periodic diffraction of electrons, projector lens to expand onto phosphor screen and image pattern allowing to users to see the image. In TEM, the monochromatic beam of electrons usually accelerated through a potential of 40- 100KV passed through a strong magnetic field .As the results, electrons are transmitted through on ultra-thin specimen interacting with the specimen as it passes through. An image is formed, magnified and focused to an

imaging devise such as layer of photographic film or detected by sensor such as camera.

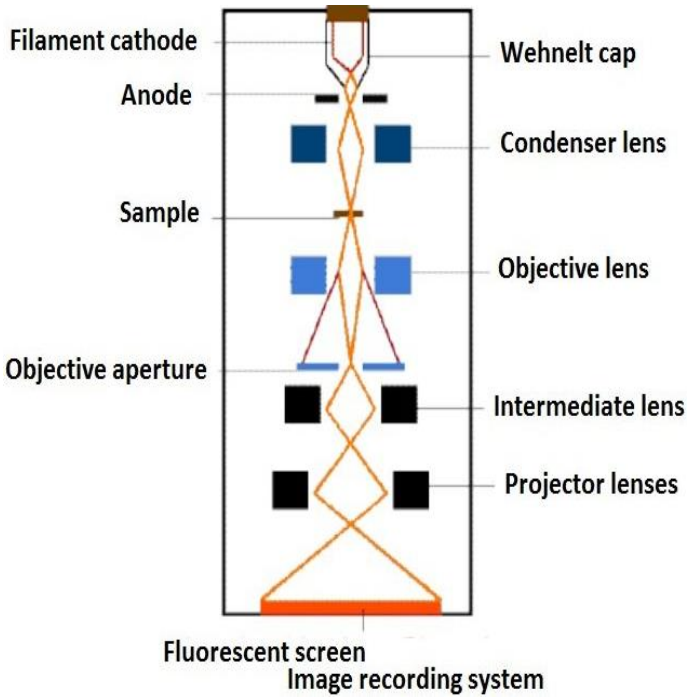

Figure 3.2 Basic of TEM and the contrast of Dislocations

The information that can be extracted by TEM depends on four parameters; the resolving power of the microscope usually smaller than 0.3 nm, the energy speed of electrons, the thickness of sample which should be less than 1μm and the composition and stability of the sample (Brydson, R., 2011). TEM is actually, provides crystallographic (morphology, size, shape arrangement of particles on scale of atomic diameter), compositional and chemical information via EDX and EELS.

3.4 UV-Vis Spectrophotometer

UV-visible spectroscopy principle is described in figure 3.3, in which a beam of light from a UV-visible light source is separated into its component

wavelengths by a prism or diffraction grating. Each monochromatic (single wavelength) beam, in turn, is split into two equal intensity beams by a half-mirrored device. One beam for the sample passes through a small transparent container (cuvette) as a sample chamber. The other beam, for reference, passes through an identical cuvette. The intensities of these light beams are then measured by electronic detectors and compared. The intensity of the reference beam, with no light absorption, is defined as I_0 and the intensity of the sample beam is defined as I, and the ratio I/I_0 is called transmittance.

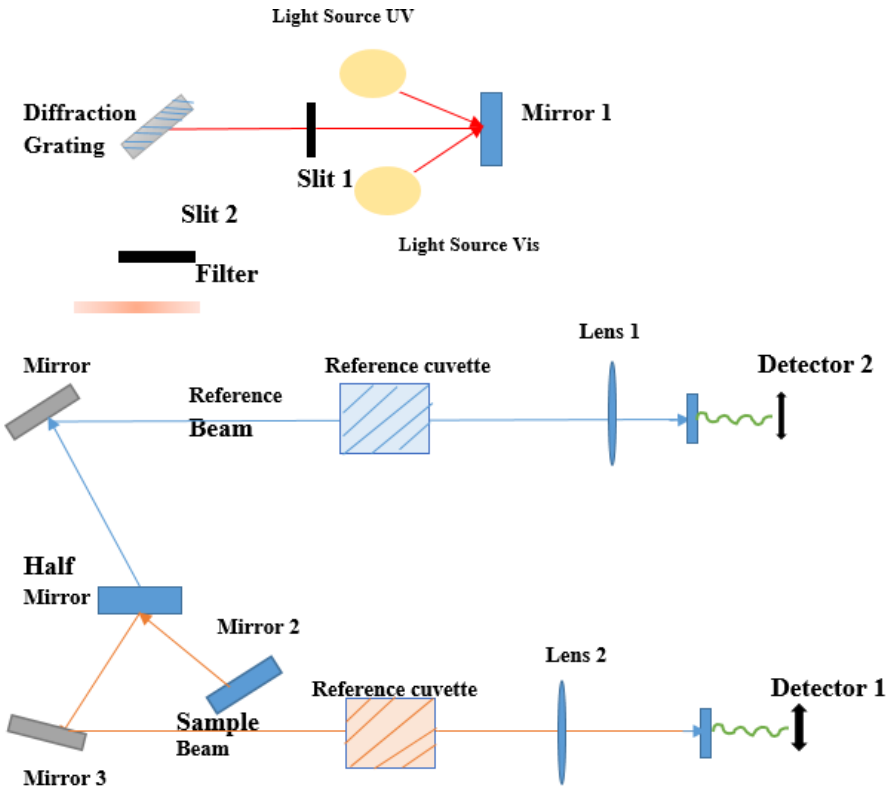

Figure 3.3 Schematic diagram of the principle of UV-visible spectroscopy and steps of taking the spectra (Smith, 1978).

Over a short period of time, the spectrometer automatically scans all the component wavelengths in the manner described. The UV region scanned normally from 200 to 400 nm, and the visible portion is from 400 to 800 nm (Osborne, 1993). If the sample compound does not absorb light of a given wavelength then $I = I_0$.

3.5 Scanning Electron Microscope (SEM)

The scanning electron microscope (SEM) is one of versatile instruments available for analysis of the chemical composition, microstructure morphology and observation of specimen surface; in this section we will present the major components of scanning electron microscope and its principle of work.

First of all, as can be seen in Figure 3.4. SEM requires an electron optical system to produce electrons and accelerated them to an energy level 0.1-30 kev, thus the electron gun is used, the diameter of the electron beam produced by hairpin tungsten gun is too large to form a high-resolution image so electromagnetic lenses and apertures are used to form a small focused electron spot on the specimen, and we have a specimen stage to place the specimen and the space surrounding it should be kept at vacuum which allows electrons to travel without scattering by the air. Also there is signal detection, electron beam scanning coils to scan the electron probe and other components, processing system provide real time observation and finally an image display unit of the specimen surface for recording (Zhou, W., 2006).

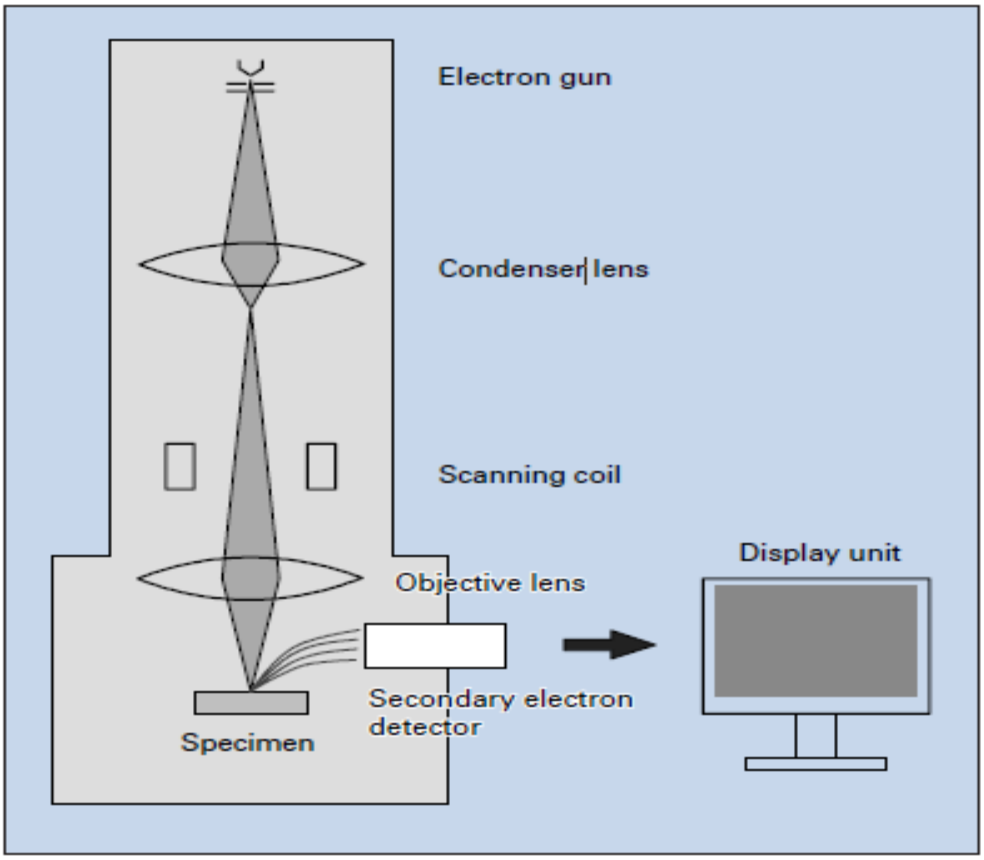

Figure 3.4 shows the basic construction of SEM

CHAPTER FOUR

RESULTS AND DISCUSIONS

4.1 Overview

Silica glass doped with silver was prepared using sol gel method. Wide range of annealing temperatures and Ag concentrations were used. Different techniques were applied to study the effect of annealing temperatures and

Ag concentrations on the formation of silver nanoparticles (Ag-NPs) in silica glass.

4.2 Structural Properties

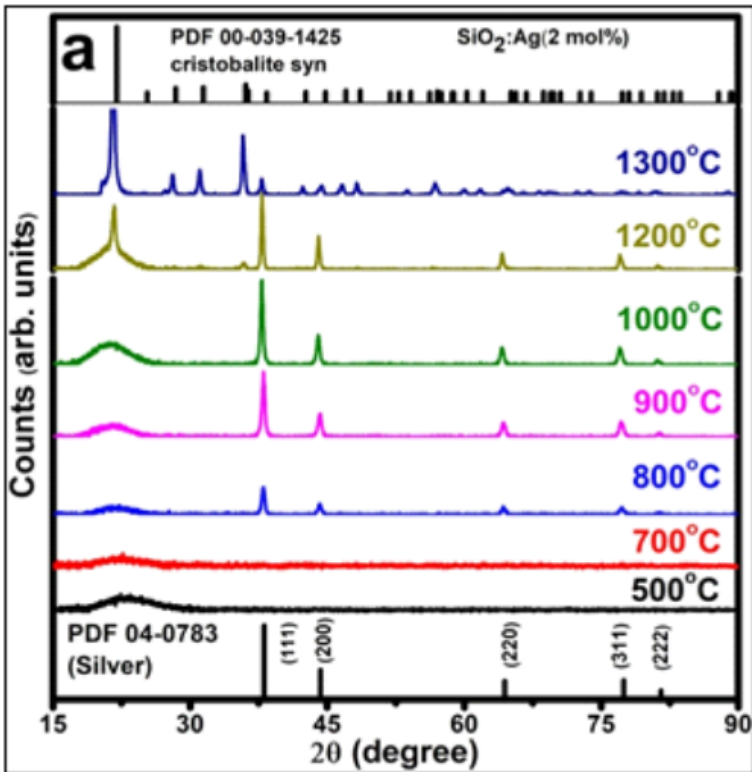

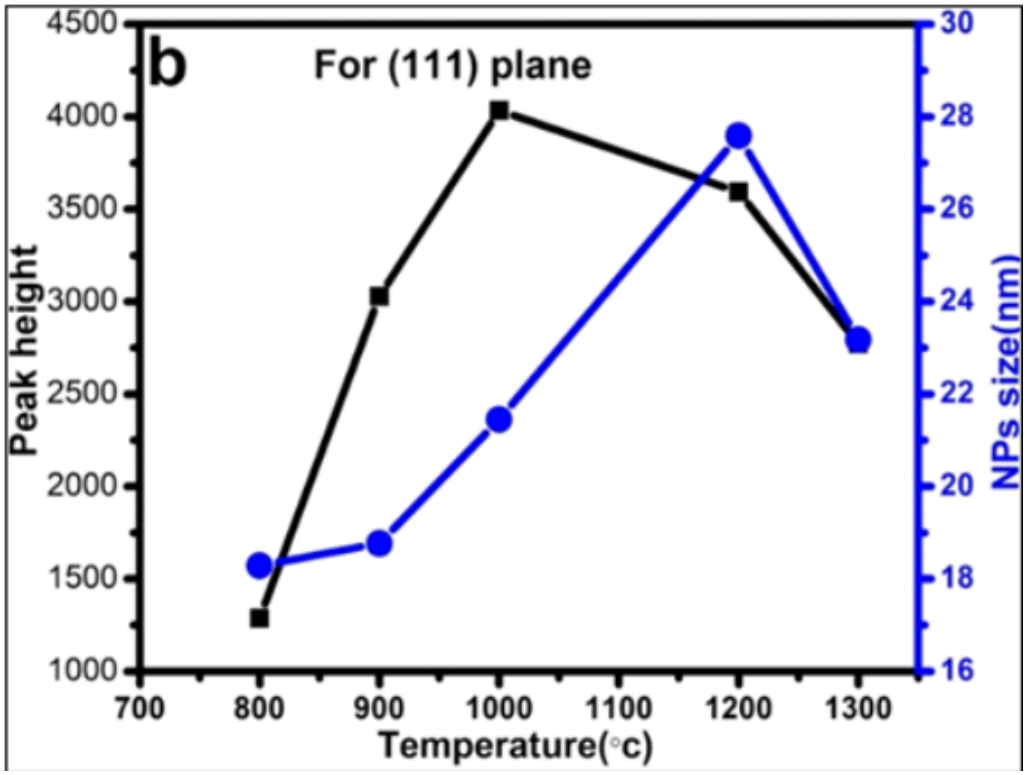

Figure 4.1 (a) XRD patterns of silica doped with 2mol%Ag annealed at different temperatures in air for 2h. (b) Peak height and particle size as the function of annealing temperature.

Figure 4.1 (a) shows XRD patterns of silica doped with 2 mol% Ag annealed at different temperatures from 500^{o}C to 1300 ^{o}C for 2h in air. As can be seen from figure 4.1 (a) there is abroad peak (hump) centered at $2\theta \approx 23^{o}$ for sample annealed at 500^{o}C, indicating the amorphous nature of the silica. This peak becomes narrower and shifted towards low angles as the annealing temperature increased and fixed at the position $2\theta \approx 21^{o}$ for samples annealed above 900^{o}C, corresponding to cristobalite phase of silica (Abbass, et al., 2017). The crystalline phase of silver did not form in samples annealed below 800 ^{o}C, indicating that the silver is in the form of ions or

small cluster (below the detection limit of XRD). Further increasing the annealing temperature to 800 ^{o}C and higher converts silver ions to silver nanoparticles as compared with the PDF file (04-0783). The following equations explain the formation of silver nanoparticles in silica (Ping-Chang, L., et al., 2014).

$$2(\equiv Si - O^{-}) \rightarrow \equiv Si - O - Si \equiv +O^{-2} \qquad (4.1)$$

$$Ag^{+} + Ag^{+} \rightarrow (Ag^{+} - Ag^{+}) \qquad (4.2)$$

$$2(Ag^{+} - Ag^{+}) + 2O^{-2} \rightarrow 4Ag^{0} + O_{2} \qquad (4.3)$$

$$Ag^{0} + Ag^{0} \rightarrow Ag\ nanoparticles \qquad (4.4)$$

Of interest is that the peak intensity of silver is become more intense with increasing the annealing temperature up to 1000^{o}C which is attributed to increase in grain size. At high annealing temperature above 1200^{o}C, the intensity was dramatically decreased. Compare to figure 4.1a, it can be seen that the increasing of Ag concentration increased the intensity peak. Thus, it can be concluded that the reduction of the peak intensity at high temperature is due decreasing of silver amount in silica. This may be due to evaporation of Ag from the surface of silica (Hui, C., et al., 2016).

Figure 4.1 (b) shows the intensity of (111) Ag peak and the average NPs size calculated using scherrer's equation (see chapter 3 section 3.2) as function of temperature. As can be seen, the particle size is increases as the annealing temperature increased up to 1200 ^{o}C and then decreased (see table 4.1) for the sample annealed at 1300^{o}C. Increasing of particle size as function of temperature may due to aggregation of nanoparticles (Jyoti, R., et al., 2013).

Table 4.1. Peak height (for 111 planes) and particle size as the function of annealing temperature calculated from figure 4.1 (a).

Annealing temperature °C	Particle size (nm)	Peak height ratio (arb.units)
800	18	1
900	19	2.4
1000	21	3
1200	28	2.8
1300	23	0.6

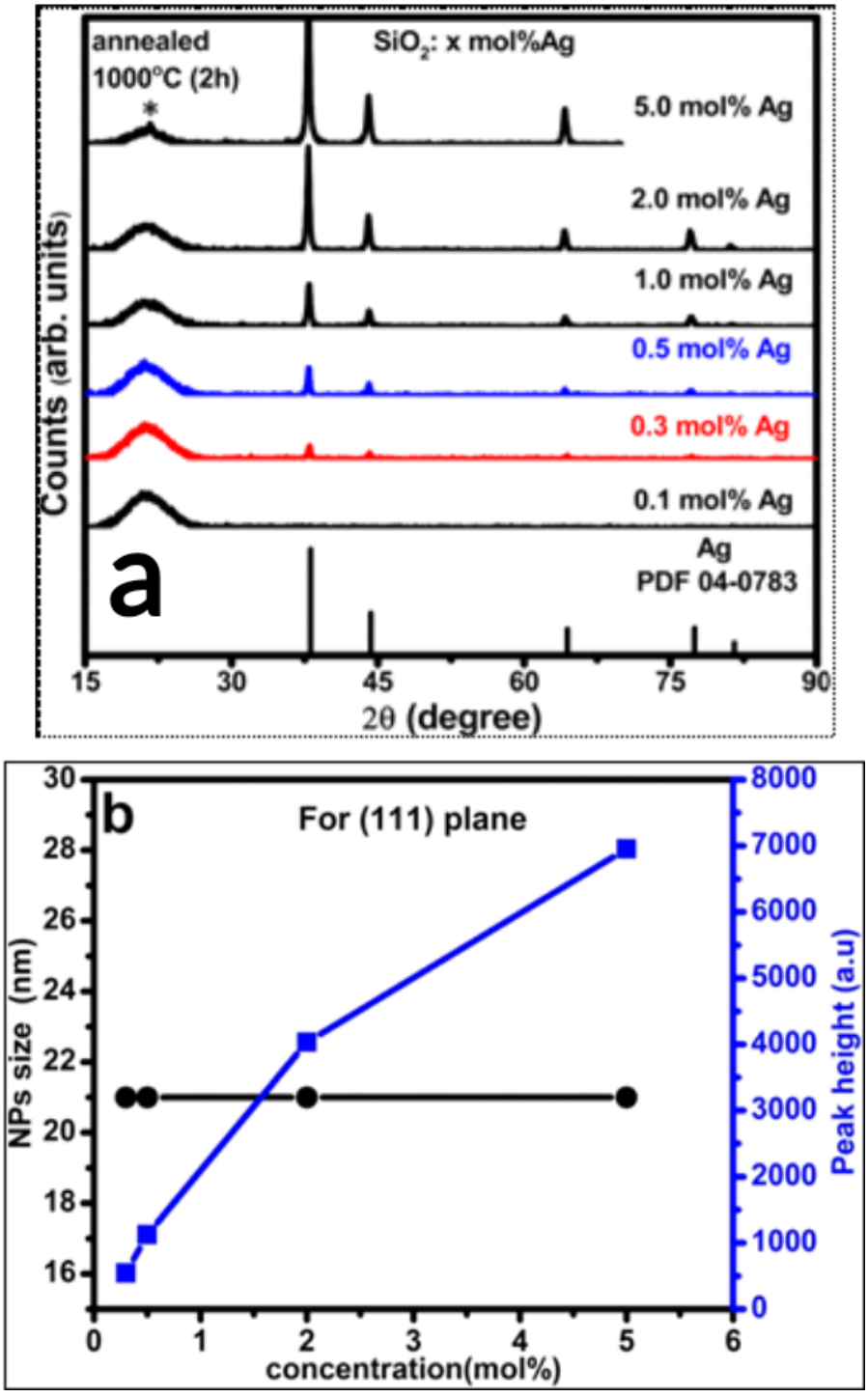

Figure 4.2 (a) XRD patterns of silica doped with different concentration of silver and annealed at 1000 ^{o}C in air for 2h. (b) Peak height and particle size as the function of silver concentration.

Figure 4.2 shows XRD patterns of silica doped with different Ag loads annealed at 1000 ^{o}C in air for 2h. Although the annealing temperature (1000^{o}C) is high enough to convert Ag ion to Ag NPs (see figure 4.1a), the sample doped with 0.1 mol% Ag did not show any peak related to Ag. This indicate that this concentration is the below detection limit of XRD. Further increased of concentration to 0.3 mol% Ag, peaks related to metallic Ag was appeared as compared with the PDF file (04-0783). The intensity of these peaks is increases as the concentration of Ag increased while the particle size remained almost unchanged (see figure 4.2b). At high concentration (5.0 mol% Ag), new peak is appeared at $2\theta \approx 21^{o}$ (marked with asterisk) which is attributed to the cristobalite phase of silica (see figure 4.2a).This peak is not shown in figure 4.1a for the sample annealed at the same temperature (1000^{o}C) but with different concentration (2mol %), which indicated that the increasing of Ag load in silica is catalyzed the structure order of amorphous silica towards the cristobalite phase.

Table 4.2. Peak height (for 111 planes) and particle size as the function of concentration calculated from figure 4.2 (a).

Concentration mol%	Particle size (nm)	Peak height ratio (arb.units)
0.5	21	1
1.0	21	2.2
2.0	21	2.8
5.0	21	13.8

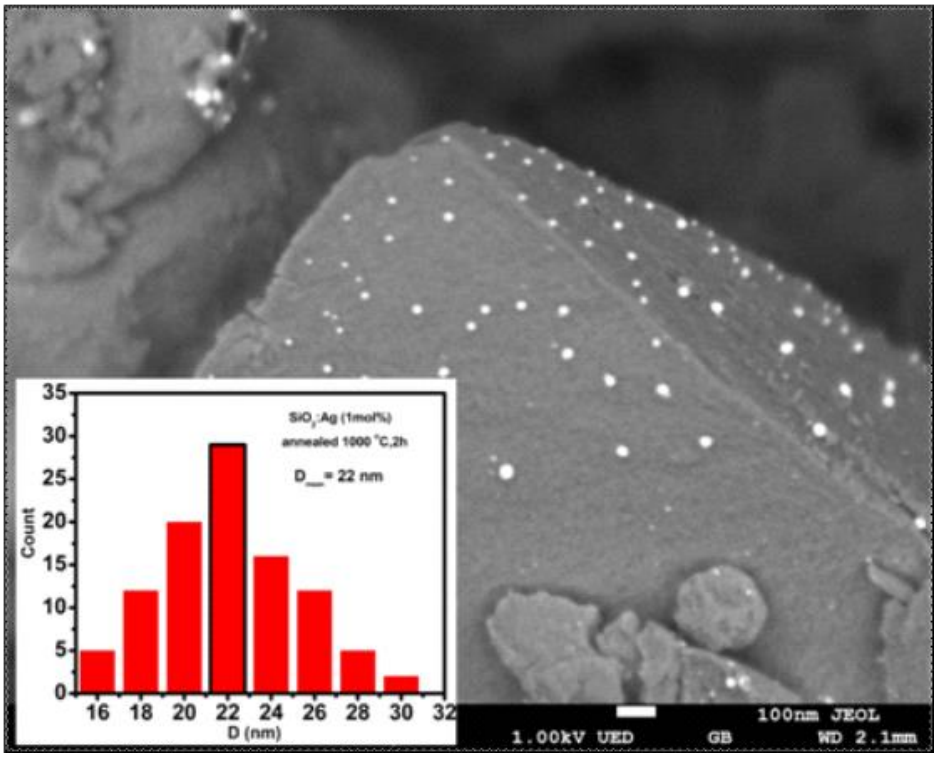

Figure 4.3 SEM image and the inset is size distribution of AgNPs for silica doped with 1mol%Ag annealed at 1000 ^{o}C for 2h.

Figure 4.3 shows a SEM image of a silica sample doped with 1 mol %Ag annealed at 1000 ^{o}C for 2h. It can be seen that the most NPs are roughly spherically in shape with the average size of 22 nm (see the inset of figure 4.3). This confirms the formation of AgNPs in silica in agreement with the XRD data. Of interest is that the average size of Ag NPs extracted from SEM is in agreement with the average size calculated by Scherrer's equation (see table 4.2). It is important to note that the AgNPs seem to be on the top surface of silica. This supports our interpretation above that at high temperature Ag NPs diffuses to the surface and then evaporated at high temperature (see figure 4.2).

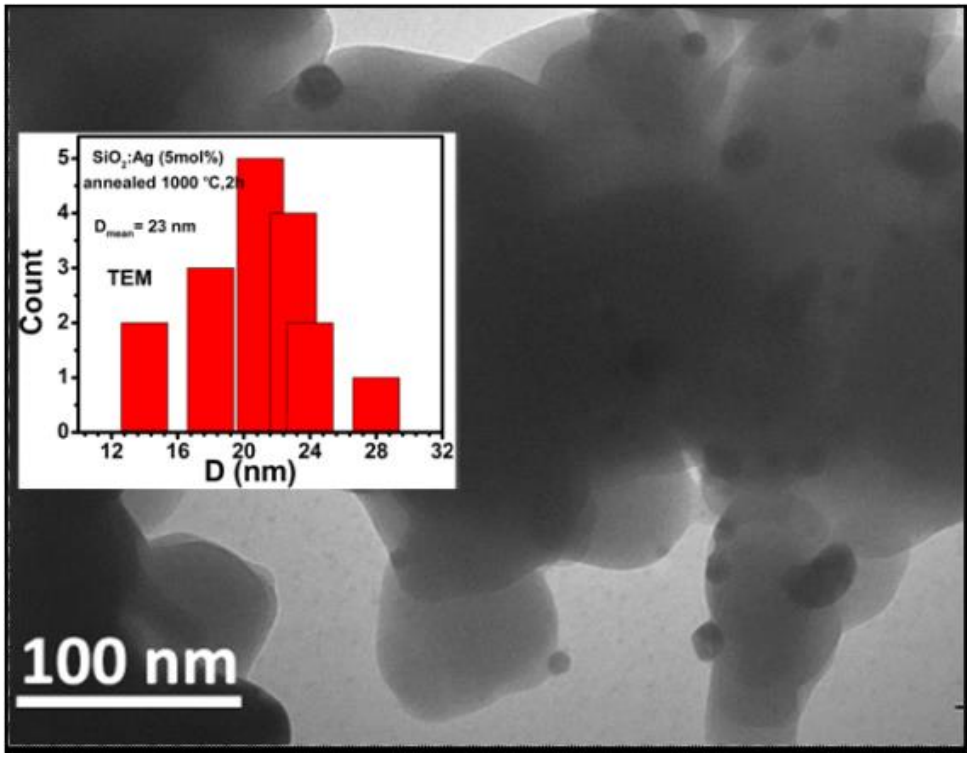

Figure 4.4 TEM image and the inset is size distribution of AgNPs for silica doped with 5mol%Ag annealed at 1000 ^{o}C for 2h.

Figure 4.4 shows TEM images of silica doped with 5 mol% Ag annealed at (a) 1000^{o}Cfor 2 h. The image shows number of Ag NPs in the silica matrix, which appear not perfectly spherical in shape and with average size about 23 nm in diameter (see the inset) in agreement with SEM and XRD. This confirms the formation of AgNPs in silica in agreement with XRD and SEM. It also confirm that the Ag concentration have no significant effect on the particle size in agreement with XRD and SEM.

4.3 Optical properties

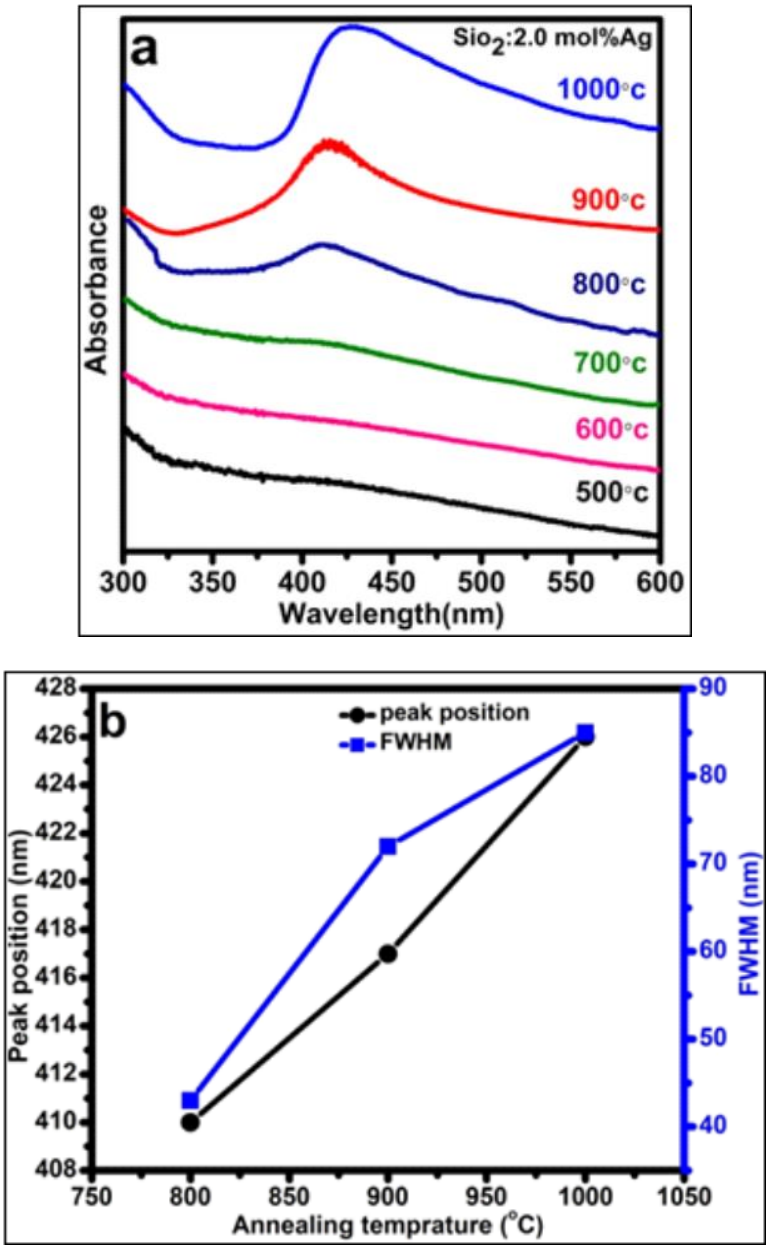

Figure 4.5 (a) UV-VIS spectrum of silica doped with 2 mol% Ag annealed at different temperatures in air in 2h. (b) Peak position and FWHM as function of annealing temperature.

Figure 4.5 (a) shows UV-VIS spectrum of silica doped with 2 mol% Ag annealed at different temperatures from 500°C to 1000°C for 2h in air. As

can be shown in figure 4.3a there is no peak appeared for samples annealed below 800°C indicating that silver aggregation or the crystalline phase for silver did not occur in agreement with XRD results (see figure 4.1a). At high annealing temperature above 800°C, abroad peak is appeared and centered at 413 nm. This peak is assigned to LSPR which confirm the formation of silver NPs (Abbass, AE., et al., 2017).

Further increasing of annealing temperature, increased the peak intensity and caused red shift in peak position. The red shift in peak position as function of annealing temperature can be assigned to the changing of particle size, since the LSPR wavelength is known to increase with increasing the particle size (see table 4.3 and table 4.1). Figure 4.5 (b) shows the effect of annealing temperature on the peak position and full width at half maximum (FWHM).

Table 4.3. Peak position and FWHM as function of annealing temperature calculated from Figure 4.3 (a).

Temperatures ^{o}C	FWHM (nm)	Position (nm)
800	44.12	413
900	71.69	424
1000	81.68	447

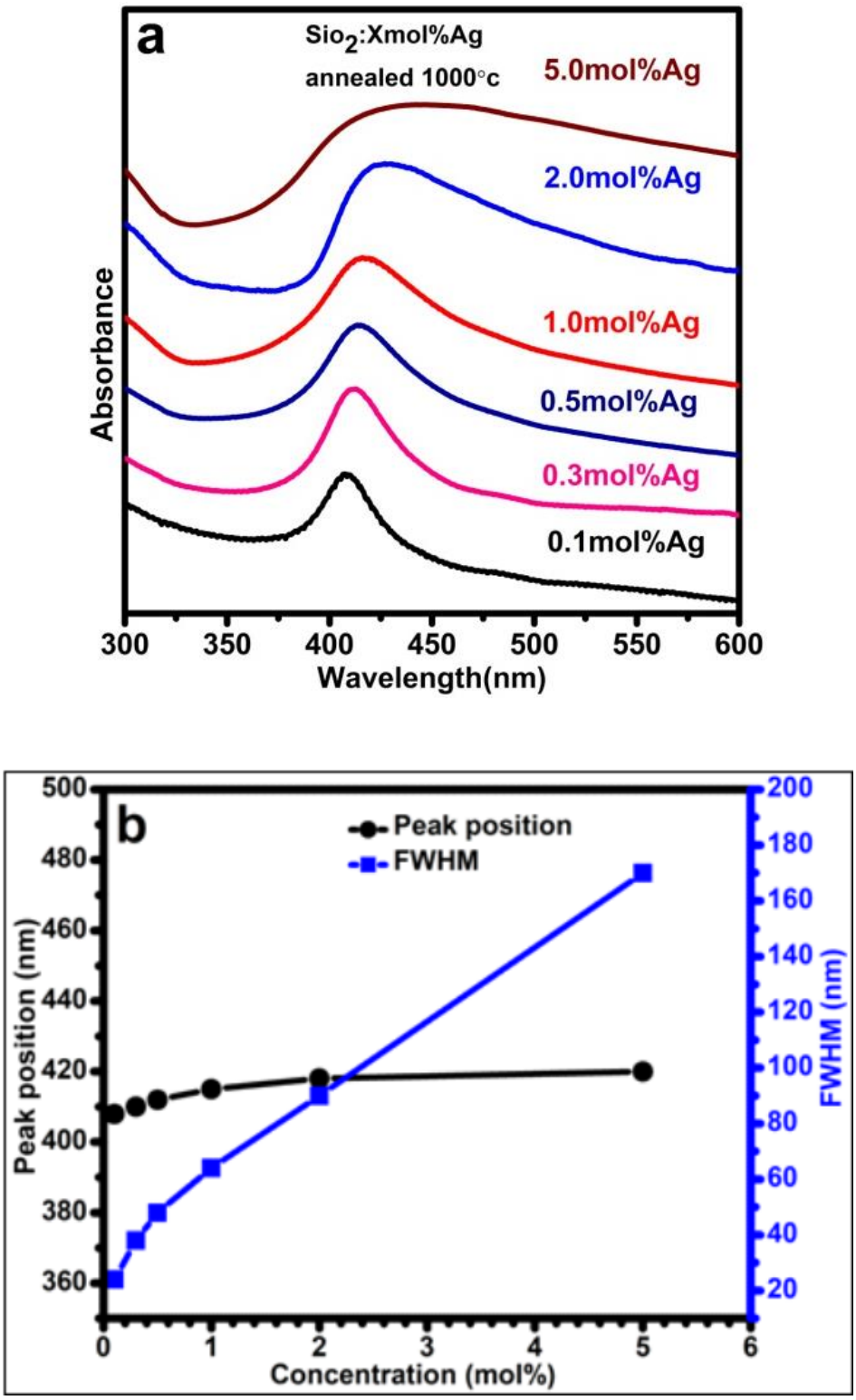

Figure. 4.6 (a) UV-VIS spectrum of silica doped with different concentrations of silver

annealed at 1000°C in air for 2h. (b) Peak position and FWHM as function of silver concentration.

Figure 4.6 (a) UV-VIS spectrum of silica doped with different Ag load at 1000°C in air for 2h. As can be seen from figure 4.6a all samples shows peaks related to LSPR which confirm the formation of Ag NPs in silica with agreement with XRD and TEM results. Of interest is that as increases of Ag load, absorption band of LSPR is broadened and small red shifted (see figure. 4.6b). It is also seen that the intensity of these peaks is dramatically increased by increasing the Ag load from 0.1 up to 1.0 mol% Ag and then decreased with further increasing in Ag load. It is reported that for large particles (≫10 nm in radius), and high distribution of particles not only the absorption band of LSPR red shift but absorption intensity also decreases (Vollmer, M. and Kreibig, U. 1995). Since XRD, TEM and SEM showed no change in particle size by increasing of silver load, therefore, the small red shift, reducing of intensity can be assigned to increasing in particle distribution.

Table 4.4 Peak position and FWHM as function of silver load calculated from Figure 4.4 (a).

Concentration mol%	FWHM (nm)	Position (nm)
0.1	31.07	410
0.3	38.08	414
0.5	48.30	418

1.0	64.14	424
2.0	77.12	443
5.0	160.32	489

.

CHAPTER FIVE

CONCLUSION AND FUTURE WORK

5.1 Conclusion

In this work, Silica doped with different amount of silver was synthesized using sol-gel method. The obtained samples were annealed at different temperatures. Different complementary techniques were used to investigate these samples. XRD, TEM, SEM and UV-VIS results confirmed the formation of silver nanoparticles in silica. The optimum concentration and annealing temperature were found to be 1mol% and between 800°C-1000°C, respectively. It can conclude that the annealing temperature can be used as mechanism to control the size of the Ag NPs in amorphous silica particularly in the range between 800°C-1000°C while silver concentration should be limited to 1mol% or less.

5.2 Recommendation

More work on the theory and experiment is needed in order to understand the formation mechanism, therefore the future work that have been left will concern about:

1. Use more techniques to emphasize the obtained results such as IR, FTIR.
2. Take the matter of time in the consideration while we are studying the impact of annealing temperature.

3. Discuss about other parameters, which can have impact in the formation of silver nanoparticles.
4. Study the impact of annealing temperature and silver concentration on other important physical and chemical properties of silver nanoparticles.

References

Abbass, AE., Vuuren, A. J., Swart, S. and Kroon, R. E. 2017. Distinguishing the nature of silver incorporated in sol-gel silica. *Journal of Non-Crystalline Solids, **475***, 71-75.

Alzoubi, F. Y. and Abu Bidier, S. A . 2013. Charcterization and aggregation of silver nanoparticles dispered in an aqueous solution. Chinese jouranal of physics, **51**, 378-387.

Andrei, A. B., Elena gabriela, U. and Hassan, Y. A. 2015. X-Ray Diffraction: Instrumentation and Applications. *Critical Reviews in Analytical Chemistry*, 289-299.

Anatoly, V. Z., Igor, I., and Alexei, A. M. 2005. Nano-optics of surface plasmon polaritons. *J Physics reports*, **408**, 131-314.

Brydson, R. (2011). Aberration-Corrected Analytical Transmission Electron Microscopy. *British Ecological society*, 296 pages.

Barbara, L. D. X-ray Powder Diffraction (XRD), Geochemical Instrumentation and Analysis. [online]. Available from https: // serc .carleton. edu /research _education/ geoche msheets/ technique s/ XRD .html [Accessed July 2018].

Carsten, S. 2001. Plasmons in metal nanostructures. PhD thesis, *Ludwig-Maximilians-University*, Germany, 134pages.

Farasat, M., Golzan, S. M. and Hassanzadeh, A. 2011. Preparation of silver nanoparticles on sol-gel base and study of their physical and morphological properties. *Iranian journal of crystallography and mineralogy*, **19**, 47-50.

Feng, W. and Ron Shen, Y .2003. General properties of local plasmons in metal nanostructures. *Physical review letters*, **97**, 1-4.

Guozhang, C. 2004. Nanostructures and nanomaterials: synthesis, properties and applications. *World scientific*, (University of Washington). Imperial College Press, 434 pages.

Hui, C., Paul, O., John, P. B., Gordon, H., Joseph, T.,and Henry, D. (2016). High-Temperature Stability of Silver Nanoparticles Geometrically Confined in the Nanoscale Pore Channels of Anodized Aluminum Oxide for SERS in Harsh Environments. *RSC Advances*,**00**,1-10.

Jyoti, R., Isha, S., Sanjeev, A. and Annu, S. 2013. Spectroscopic Analysis Of Ag Nanoparticles Embedded In Glass. *Advanced Materials Letters*, ***4***(8), 598-604.

Jose, R. M., Jose, L. E., Alejandra, C., Katherine, H., Juan, B. K., Jose Tapia, R. Miguel, J.Y. 2005. The bactericidal effect of silver nanoparticles. *J. Nanotechnology*. Nanotechnology, **16**, 2346–235.

Kamal, K. P. and Pravat, K. G. 2017. Plasmonic Metal and Semiconductor Nanoparticle Decorated TiO2-Based Photocatalysts for Solar Light Driven Photocatalysis. In book: Reference Module in Chemistry, Molecular Sciences and Chemical Engineering, *Elsevier*, *Intech*, 786-794.

Mauro, E., Cinzia, G., Leander, T. and Lorenzo, V. 2000. Sol–gel synthesis and characterization of Ag and Au nanoparticles in SiO_2, TiO_2, and ZrO_2 thin films. *Journal of the American Ceramic Society*, **83**, 2385–2393.

Mahltig, B., Gutmann, E., Reibold, M., Meyer, D. C. and Bottcher, H. 2009. Synthesis of Ag and Ag/SiO2 sols by solvothermal method and their bactericidal activity. *Journal of Sol-Gel Science and Technology*, ***51***(2), 204-214.

Matthew, R., Claire, M. C., Weiyang, L., Christine, H. M., Qiang, Z., Dong, Q.and Younan, X. 2011. Controlling the synthesis and assembly of silver nanostructures for plasmonic applications, *Chemical Reviews*, **111**, 3669-3712.

Matthew, E. S., Christopher, R. A., Lucas B. T., Joana, M., Stephen, K. G., John, A. R. and Ralph G. N .2008. Nanostructured plasmonic sensors. *J Chemical reviews*, **108**, 494−521.

Nicholas, J. B. 2011. Optical structure-property relations in metal and semiconductor nanoparticles. PhD dissertation, *The University of Utah*, 170 pages.

Ning, S. 2012. Synthesis, characterization and optical properties of hybrid nanoparticles working with plasmon-fluorescence coupling. PhD. *Ecole Centrale de Lyon,* France.

Ojeda-MartÍnez, M. L., Yanez-Sánchez, I., Zamudio-Ojedab, A., Gálvez-Gastelum, F.J., Machuca-Gonzálezb, R. and Velásquez-Ordońez, C. 2013. SiO2-Ag generation bu sol-del technique for antibacterial use. Digest Journal of Nanomaterials and Biostructures, **8**, 409 – 414.

Osborne .1993. Practical Nir Spectroscopy With Applications in Food and Beverage Analysis. *Addison-Wesley Longman Ltd*.

Ping-Chang, L., Stephen, L., Paul, C.W. and Rajagopalan, S. 2014. Techniques for physicochemical characterization of nanomaterials. *Biotechnology Advances, **32**,* 711-726.

Prema, P. 2011. Chemical Mediated Synthesis of Silver Nanoparticles and its Potential Antibacterial Application. In book: *on Molecular and Environmental Bioengineering - From Analysis and Modeling to Technology Applications*, edited by Carpi, A, *Intech*, 1-203.

Poppe, L. J., Paskevich, V.F. , Hathaway, J.C. and Blackwood, D.S. 2001. A laboratory manual for X-ray powder diffraction. *US Geological Survey open-file report* [online]. Available from https: // pubs .usgs .gov/of/2001/of01-041/ [Accessed July 2018].

Renata, R., Viktoria, L. and Tsiala, S. 2011. Interaction of luminescent dyes with noble metal nanoparticles in organic–inorganic glasses for future luminescent materials. *Polymers for Advanced Technologies*, **22**, 60-64.

Rivera, V.A.G., Ferri, F.A. and Marega, E. 2012. Localized Surface Plasmon Resonances: Noble Metal Nanoparticle Interaction with Rare-Earth Ions: In book *Plasmonics - Principles and Applications*, edited by Kim, K. Y., *Intech*, *283-312*.

Stefan, K., Bernd, H. G., Ralf, H. and Helmut S. 1997. Study of isotropically conductive bondings filled with aggregates of nano-sited Ag-particles. J. *IEEE Transactions on Components, Packaging & A, Manufacturing Technology*, **20**, 15-20.

Salem, M. 2018. Effect of Size, Shape and Environment on the Optical Response of Metallic Nanoparticles: In book *Noble and Precious*

Metals - Properties, Nanoscale, edited by Seehra, M., Singh, B. and Alan D., *Intech Open*, 43-64.

Sukdeb, P., Yu Kyung, T. and Joon, M. S .2007. Does the antibacterial activity of silver nanoparticles depend on the shape of the nanoparticle? A study of the gram-negative bacterium Escherichia coli. *J Applied and environmental microbiology*. **73**, 712–1720.

Smith. 1978. Carbon-13 NMR spectroscopy of steroids Annual Reports on NMR Spectroscopy. *Elsevier*.

Tanja, K., Ralph, J., Eva, O. and Claes-Göran, G. 2001. Bacteria as workers in the living factory: metal-accumulating bacteria and their potential for materials science. *TRENDS in Biotechnology*, **19**, 15-29.

Vincenzo, A., Roberto, P., Marco, F., Onofrio, M. M. and Maria, A. I .2017. Surface plasmon resonance in gold nanoparticles. *Journal of Physics Condensed Matter*, **29**, 1-48.

Vollmer, M. and Kreibig, U. 1995. Optical properties of metal clusters. *Springer Series in Materials Science*, **25**, 28-88.

Xianmao, L., Matthew, R., Sara, E. S., Benjamin, W. and Younan, X .2009. Chemical synthesis of novel plasmonic nanoparticles. *J Annual review of physical chemistry*, **60**. 167-192.

Zhou, W., Apkarian, R., Wang, Z.L., Joy, D. 2006. Fundamentals of Scanning Electron Microscopy (SEM). In: Zhou W., Wang Z.L. (eds) Scanning Microscopy for Nanotechnology. *Springe*r, New York. 1-40.